it is undoubtedly crystalline, having plane faces and sharp edges and giving an X-ray diffraction pattern and yet approximately two-thirds of its volume is occupied essentially by liquid.

When the crystals of Cu[4,4',4'',4'''-tetracyanotetraphenylmethane]$BF_4 \cdot x C_6H_5NO_2$ were collected from the reaction mixture, washed with nitrobenzene, and dried a stream of air until a free-running solid was obtained, the IR spectrum (KBr disk) of the solid so obtained showed a very sharp $\nu_{C\equiv N}$ at 2240 cm^{-1}, major nitrobenzene bands at 705, 1345, and 1520 cm^{-1}, and a strong BF_4^- band at 1060 cm^{-1}. Positions of minor bands arising from the tetranitrile moiety and from the nitrobenzene were very similar to those observed for the tetranitrile alone (KBr disk) and nitrobenzene alone (liquid film). The crystals appeared, under the microscope, to retain their external faces and edges and their internal transparency after suspension in a solution of NBu_4PF_6 (large excess) in nitrobenzene. However, the IR spectrum of the crystals after such treatment showed complete replacement of the initially strong BF_4^- band at 1060 cm^{-1} by an intense band at 830 cm^{-1} together with a medium band at 560 cm^{-1}, both associated with PF_6^-, the rest of the spectrum being essentially unchanged.

Conclusions

It is very likely that interpenetration of independent 3D frameworks of the sort observed for the archetypal $Zn(CN)_2$, and possibly of other types that can be envisaged, will be a major concern in future attempts to construct scaffolding structures with more complex rods. The deliberate construction of a single diamond-related framework in $[N(CH_3)_4][CuZn(CN)_4]$ demonstrates the potential usefulness of simple metal cyanides for the exploration of some of the possible factors influencing or controlling interpenetration. The first deliberately designed material constructed from rods of some complexity, namely, Cu[4,4',4'',4'''-tetracyanotetraphenylmethane]$BF_4 \cdot x C_6H_5NO_2$ proves to be unusual, approximately one-third of its volume consisting of an ordered framework which imposes crystallinity on the substance, the other two-thirds being essentially liquid. There is currently much interest in widening the range of the potential catalytic applications of zeolites by synthesizing new examples with larger pores and cavities. We note that the small fraction of space occupied by the Cu-tetranitrile framework in the present example compares most favorably in this respect with available zeolites. This particular framework was designed with the prime purpose of demonstrating general possibilities in a way that combined synthetic simplicity with likelihood of success. A wide range of general synthetic approaches to a variety of different frameworks are presented here. On the basis of this preliminary work the prospects look good for generating many new, unusual and possibly useful materials.

Acknowledgment. We thank Mr. Lu Zhenrong for assistance with the X-ray study of $[N(CH_3)_4][CuZn(CN)_4]$.

Supplementary Material Available: Tables S-I to S-IV listing observed and calculated structure factors for $Zn(CN)_2$, $Cd(CN)_2$, $[N(CH_3)_4][CuZn(CN)_4]$, and Cu[4,4',4'',4'''-tetracyanotetraphenylmethane]$BF_4 \cdot x C_6H_5NO_2$ ($x \geq 7.7$) (7 pages). Ordering information is given on any current masthead page.

(μ-Oxo)(μ-carboxylato)diiron(III) Complexes with Distinct Iron Sites. Consequences of the Inequivalence and Its Relevance to Dinuclear Iron-Oxo Proteins

Richard E. Norman,[†] Shiping Yan,[†,1] Lawrence Que, Jr.,*[,†] Gabriele Backes,[‡] Jinshu Ling,[‡] Joann Sanders-Loehr,*[,‡] Jian H. Zhang,[§] and Charles J. O'Connor[§]

Contribution from the Department of Chemistry, University of Minnesota, Minneapolis, Minnesota 55455, Department of Chemical and Biological Sciences, Oregon Graduate Center, Beaverton, Oregon 97006-1999, and Department of Chemistry, University of New Orleans, New Orleans, Louisiana 70122. *Received July 17, 1989*

Abstract: A new family of (μ-oxo)(μ-carboxylato)diiron(III) complexes has been synthesized with use of the tetradentate tripodal ligand tris(2-pyridylmethyl)amine (TPA) with benzoate, acetate, and diphenyl phosphate as bridging ligands. $[Fe_2(TPA)_2O(OBz)](ClO_4)_3 \cdot 2H_2O$ crystallizes in the monoclinic space group $P2_1/n$ with a = 11.669 (15) Å, b = 19.568 (20) Å, c = 22.285 (12) Å, and β = 102.24 (8)°. The structure was determined at -84 °C from 5445 out of a total of 8854 reflections with R = 0.064 and R_w = 0.080. $[Fe_2(TPA)_2O(OAc)](ClO_4)_3 \cdot H_2O \cdot (CH_3COCH_3)$ crystallizes in the monoclinic space group $P2_1/n$ with a = 20.774 (46) Å, b = 22.312 (5) Å, c = 10.372 (7) Å, and β = 104.14 (12)°. The structure was determined at -88 °C from 6324 out of a total of 9147 reflections with R = 0.078 and R_w = 0.091. $[Fe_2(TPA)_2O(O_2P\{OPh\}_2)](ClO_4)_3(CH_3COCH_3)$ crystallizes in the triclinic space group $P\bar{1}$ with a = 11.82 (1) Å, b = 13.32 (1) Å, c = 18.03 (1) Å, α = 92.67 (5)°, β = 94.48 (5)°, and γ = 94.22 (5)°. The structure was determined at -83 °C from 6931 out of a total of 9885 reflections with R = 0.049 and R_w = 0.061. These crystal structures establish the presence of a doubly bridged diiron core with distinct iron sites. On one iron, the amine nitrogen of TPA is trans to the oxo bridge, while one of the pyridines is trans to the oxo bridge on the other iron. These complexes exhibit electronic and Mössbauer spectral features and magnetic properties that are very similar to those of (μ-oxo)diiron(III) proteins as well as (μ-oxo)bis(μ-carboxylato)diiron(III) complexes, demonstrating that these properties are not significantly affected by the number of carboxylate bridges and the inequivalence of the iron sites. The iron(III) sites remain distinct in solution as evidenced by ^1H NMR and resonance Raman spectroscopies. The inequivalence is manifested in the resonance Raman spectra as an enhancement of the ν_{as}(Fe-O-Fe) intensity, which is comparable to those found for (μ-oxo)diiron(III) proteins such as methemerythrin and ribonucleotide reductase.

The (μ-oxo)bis(μ-carboxylato)diiron(III) unit is well established in the structure of hemerythrin in its met and oxy forms.[2] The active site of this invertebrate dioxygen carrier has been the focus of an intense modeling effort by several groups with a variety of

[†] University of Minnesota.
[‡] Oregon Graduate Center.
[§] University of New Orleans.

(1) Visiting scientist from Nankai University, Tianjin, People's Republic of China.

0002-7863/90/1512-1554$02.50/0

Table I. Crystal Structure Parameters of TPA Complexes

	1	2	3
empirical form	$C_{43}H_{45}Cl_3Fe_2N_8O_{17}$	$C_{40}H_{45}Cl_3Fe_2N_8O_{17}$	$C_{51}H_{52}Cl_3Fe_2N_8O_{18}P$
fw	1163.93	1127.89	1314.04
lattice param			
a (Å)	11.669 (15)	20.774 (46)	11.82 (1)
b (Å)	19.568 (20)	22.312 (5)	13.32 (1)
c (Å)	22.285 (12)	10.372 (7)	18.03 (1)
α (deg)	90.0	90.0	92.67 (5)
β (deg)	102.24 (8)	104.14 (12)	94.48 (5)
γ (deg)	90.0	90.0	94.22 (5)
V (Å^3)	4973 (16)	4662	2818 (7)
space group	$P2_1/n$ (No. 14)	$P2_1/n$ (No. 14)	$P\bar{1}$ (No. 2)
Z	4	4	2
D_{calc} (g cm^{-3})	1.554	1.607	1.548
μ (cm^{-1})	8.21	8.73	7.62
radiation		Mo Kα (λ = 0.71069 Å)	
temp (°C)	−84	−88	−83
residuals:[a] R, R_w	0.064, 0.080	0.078, 0.091	0.049, 0.061

[a] $R = \sum||F_o| - |F_c||/\sum|F_o|$; $R_w = [(\sum w(|F_o| - |F_c|)^2/\sum wF_o^2)]^{1/2}$.

tridentate amine ligands.[3-6] The physical characterization of various methemerythrins[7] and model complexes[3-6,8-12] has afforded a large body of data for comparison and defined the intrinsic properties of this dinuclear unit. It is clear that the oxo bridge gives rise to short Fe–O_{oxo} bonds, strong antiferromagnetic coupling, and large Mössbauer quadrupole splittings. The presence of the carboxylate bridges constrains the Fe–O–Fe angle to 120 ± 5° and the Fe···Fe separation to 3.1 ± 0.1 Å. The (μ-oxo)diiron(III) unit also exhibits symmetric and asymmetric Fe–O–Fe resonance Raman vibrations, with spectral intensities that depend on the coordination environment of the dinuclear unit.[13]

The dinuclear iron unit of the ribonucleotide reductase from *Escherichia coli* exhibits all of the above characteristics.[14,15] This similarity to methemerythrin has led to speculation that the former may have such a (μ-oxo)bis(μ-carboxylato)diiron core.[4,15] However, the presence of this core has not been unequivocally demonstrated, since the crystal structure of the protein has yet to be solved.[16] The dinuclear iron protein purple acid phosphatase is another candidate for the (μ-oxo)diiron(III) category.[15,17] Although it exhibits the expected magnetic[18] and Mössbauer properties[18,19] as well as an Fe···Fe separation[15,20] of ≤3.2 Å, Raman[18] and EXAFS[15,20] evidence for an Fe–O–Fe moiety is still lacking.

We have discovered that the use of tetradentate tripodal ligands in place of tridentate ligands favors the formation of dibridged Fe–O–Fe complexes instead of the tribridged analogues. The first member of this series was prepared from the ligand *N*-(2-hydroxybenzyl)-*N*,*N*-bis(2-pyridylmethyl)amine (HDP)[21] to yield the (μ-oxo)(μ-carboxylato) complex[22] $[Fe_2(HDP)_2O(OBz)]^+$. Due to the presence of a phenolate ligand in HDP, this complex serves as a model for the iron–tyrosinate active site of the purple acid phosphatases. Substitution of the tetradentate amine ligand tris(2-pyridylmethyl)amine (TPA) led to the formation of the $[Fe_2(TPA)_2O(OBz)](ClO_4)_3$ (**1**)[23] complex,[24] with the surprising result that the complex had assembled in an unsymmetric fashion yielding two distinct iron sites. The structures of the corresponding acetate- and phosphate-bridged complexes, $[Fe_2(TPA)_2O(OAc)](ClO_4)_3$ (**2**)[23] and $[Fe_2(TPA)_2O(O_2P\{OPh\}_2)](ClO_4)_3$ (**3**),[23] have been determined to contain the analogous core-retaining distinct iron sites. The consequences of the single carboxylate bridge and the presence of inequivalent iron sites on the structure and spectroscopy of the (μ-oxo)diiron unit are assessed in this paper. In particular, the TPA complexes exhibit Raman properties that more closely mimic those of hemerythrin and ribonucleotide reductase in their Fe^{III}_2 forms than previously reported model complexes.

(2) Stenkamp, R. E.; Sieker, L. C.; Jensen, L. H. *J. Am. Chem. Soc.* **1984**, *106*, 618–622.
(3) (a) Chaudhuri, P.; Wieghardt, K.; Nuber, B.; Weiss, J. *Angew. Chem., Int. Ed. Engl.* **1985**, *24*, 778–779. (b) Hartman, J. R.; Rardin, R. L.; Chaudhuri, P.; Pohl, K.; Wieghardt, K.; Nuber, B.; Weiss, J.; Papaefthymiou, G. C.; Frankel, R. B.; Lippard, S. J. *J. Am. Chem. Soc.* **1987**, *109*, 7387–7396.
(4) Armstrong, W. H.; Spool, A.; Papaefthymiou, G. C.; Frankel, R. B.; Lippard, S. J. *J. Am. Chem. Soc.* **1984**, *106*, 3653–3667.
(5) Toftlund, H.; Murray, K. S.; Zwack, P. R.; Taylor, L. F.; Anderson, O. P. *J. Chem. Soc., Chem. Commun.* **1986**, 191–193.
(6) Gomez-Romero, P.; Casan-Pastor, N.; Ben-Hussein, A.; Jameson, G. B. *J. Am. Chem. Soc.* **1988**, *110*, 1988–1990.
(7) (a) Klotz, I. M.; Kurtz, D. M., Jr. *Acc. Chem. Res.* **1984**, *17*, 16–22. (b) Sanders-Loehr, J. In *Iron Carriers and Iron Proteins*; Loehr, T. M., Ed.; VCH Publishers: New York, 1989; pp 373–466.
(8) (a) Armstrong, W. H.; Lippard, S. J. *J. Am. Chem. Soc.* **1985**, *107*, 3730–3731. (b) Turowski, P. N.; Armstrong, W. H.; Roth, M. E.; Lippard, S. J. *J. Am. Chem. Soc.*, in press.
(9) Drüeke, S.; Wieghardt, K.; Nuber, B.; Weiss, J.; Fleischhauer, H.-P.; Haase, W. *J. Am. Chem. Soc.* **1989**, *111*, 8622–8631.
(10) Vincent, J. B.; Huffman, J. C.; Christou, G.; Li, Q.; Nanny, M. A.; Hendrickson, D. N.; Fong, R. H.; Fish, R. H. *J. Am. Chem. Soc.* **1988**, *110*, 6898–6900.
(11) Chen, Q.; Lynch, J. B.; Gomez-Romero, P.; Ben-Hussein, A.; Jameson, G. B.; O'Connor, C. J.; Que, L., Jr. *Inorg. Chem.* **1988**, *27*, 2673–2681.
(12) Murch, B. P.; Bradley, F. C.; Que, L., Jr. *J. Am. Chem. Soc.* **1986**, *108*, 5027–5028.
(13) Sanders-Loehr, J.; Wheeler, W. D.; Shiemke, A. K.; Averill, B. A.; Loehr, T. M. *J. Am. Chem. Soc.* **1989**, *111*, 8084–8093.
(14) Reichard, P.; Ehrenberg, A. *Science (Washington, D.C.)* **1983**, *221*, 514–519.
(15) Que, L., Jr.; Scarrow, R. C. *ACS Symp. Ser* **1988**, *No. 372*, 152–178.
(16) Joelson, T.; Uhlin, U.; Eklund, H.; Sjöberg, B.-M; Reichard, P. *J. Biol. Chem.* **1984**, *259*, 9076–9077.
(17) Doi, K.; Antanaitis, B. C.; Aisen, P. *Struct. Bonding (Berlin)* **1988**, *70*, 1–26.
(18) Averill, B. A.; Davis, J. C.; Burman, S.; Zirino, T.; Sanders-Loehr, J.; Loehr, T. M.; Sage, J. T.; Debrunner, P. G. *J. Am. Chem. Soc.* **1987**, *109*, 3760–3767.
(19) Debrunner, P. G.; Hendrich, M. P.; DeJersey, J.; Keough, D. T.; Sage, J. T.; Zerner, B. *Biochim. Biophys Acta* **1983**, *745*, 103–106.
(20) (a) Kauzlarich, S. M.; Teo, B. K.; Zirino, T.; Burman, S.; Davis, J. C.; Averill, B. A. *Inorg. Chem.* **1986**, *25*, 2781–2785. (b) Scarrow, R. C.; Que, L., Jr. Manuscript in preparation.
(21) The following abbreviations are used throughout: HDP, *N*-(2-hydroxybenzyl)-*N*,*N*-bis(2-pyridylmethyl)amine; TPA, tris(2-pyridylmethyl)amine; Me_3tacn, *N*,*N*′,*N*″-trimethyl-1,4,7-triazacyclononane; $HB(pz)_3$, hydrotris(pyrazolyl)borate; BPA, bis(2-pyridylmethyl)amine; BBA, bis(2-benzimidazolylmethyl)amine; tpbn, *N*,*N*,*N*′,*N*′-tetrakis(2-pyridylmethyl)-1,4-diaminobutane; 5,6-Me_2HPTB, *N*,*N*,*N*′,*N*′-tetrakis[(5,6-dimethyl-2-benzimidazolyl)methyl]-2-hydroxy-1,3-diaminopropane; bipy, 2-2′-bipyridine; N5, *N*,*N*,*N*′-tris(2-benzimidazolyl)methyl)-*N*′-(2-hydroxyethyl)-1,2-diaminoethane; tmip, tris(*N*-methyl-2-imidazolyl)phosphine; and tpbn, *N*,*N*,*N*′,*N*′-tetrakis(2-pyridylmethyl)-1,4-diaminobutane.
(22) Yan, S.; Que, L., Jr.; Taylor, L. F.; Anderson, O. P. *J. Am. Chem. Soc.* **1988**, *110*, 5222–5224.
(23) Although these complexes can be crystallized in various solvated forms (i.e., complex·2H_2O, complex·2(CH_3COCH_3), etc.), the solvent molecules are lost upon dissolution. To avoid confusion, we use the following scheme and ignore the state of solvation throughout the text: **1**, $[Fe_2(TPA)_2O(OBz)](ClO_4)_3$; **2**, $[Fe_2(TPA)_2O(OAc)](ClO_4)_3$; **3**, $[Fe_2(TPA)_2O(O_2P\{OPh\}_2)](ClO_4)_3$.
(24) Yan, S.; Cox, D. D.; Pearce, L. L.; Juarez-Garcia, C.; Que, L., Jr.; Zhang, J. H.; O'Connor, C. J. *Inorg. Chem.* **1989**, *28*, 2507–2509.

Experimental Procedures

Synthetic Methods. TPA·$HClO_4$ and TPA·$3HClO_4$ were synthesized according to literature procedures,[25,26] while all other chemicals were purchased commercially and used as received. *Caution*: The perchlorate salts in this study are all potentially explosive and should be handled with care.

The various $[Fe_2(TPA)_2O(L)](ClO_4)_3$ complexes are all prepared similarly. A typical preparation of **1** is as follows: TPA·$3HClO_4$ (0.5917 g, 1.0 mmol) was dissolved in 40 mL of MeOH and treated with Et_3N (0.63 mL, 4.5 mmol). $Fe(ClO_4)_3·10H_2O$ (0.5366 g, 1.0 mmol) in a small volume (1–2 mL) of MeOH was added to the resulting solution of TPA. To this resultant red solution was added NaOBz (0.0723 g, 0.5 mmol). The solution turns green/brown over a couple of minutes, followed by the precipitation of **1** as a green/brown powder. The complex can be crystallized either by filtering the methanol solution and allowing the filtrate to stand in an ethyl acetate bath or by dissolving the green/brown powder in acetone and allowing the resulting solution to stand in a bath of ethyl acetate. Crystals are deposited over a period of days (yield 0.4207 g, 73%). This scheme affords other complexes that are crystalline materials and afford satisfactory elemental analyses. Anal. Calcd for $[Fe_2(TPA)_2O(OBz)](ClO_4)_3$ ($C_{43}H_{41}Cl_3Fe_2N_8O_{15}$): C, 45.78; H, 3.64; N, 9.94; Cl, 9.45. Found: C, 45.75; H, 3.83; N, 9.71; Cl, 9.19.

Substitution of NaOAc for NaOBz in the above preparation gives **2**. Anal. Calcd for $[Fe_2(TPA)_2O(OAc)](ClO_4)_3·2H_2O$ ($C_{38}H_{43}Cl_3Fe_2N_8O_{17}$): C, 41.42; H, 3.93; N, 10.17; Cl, 9.65. Found: C, 41.32; H, 3.93; N, 9.84; Cl, 9.81. Anal. Calcd for $[Fe_2(TPA)_2O(OAc)](ClO_4)_3·H_2O·(CH_3COCH_3)$ ($C_{41}H_{47}Cl_3Fe_2N_8O_{17}$): C, 43.12; H, 4.15; N, 9.81. Found: C, 42.96; H, 4.38; N, 10.04.

Substitution of $HOP(O)\{OPh\}_2$ and 1 equiv of Et_3N for NaOBz in the above preparation gives **3**. Anal. Calcd for $[Fe_2(TPA)_2O(O_2P\{OPh\}_2)](ClO_4)_3·2(CH_3COCH_3)$ ($C_{54}H_{58}Cl_3Fe_2N_8O_{19}P$): C, 47.27; H, 4.26; N, 8.17; P, 2.26; Cl, 7.75. Found: C, 46.98; H, 4.61; N, 8.49; P, 2.19; Cl, 7.67.

The preparation of $[Fe_2(HDP)_2O(OBz)](BPh_4)$ (**4**) has been described previously.[22]

$[Fe_2(BPA)_2O(OBz)_2](ClO_4)_2·H_2O$ (**11**) is prepared by the following procedure: A solution of BPA (0.400 g, 2.0 mmol) in 10 mL of EtOH was added to a solution containing $Fe(ClO_4)_3·10H_2O$ (0.744 g, 1.4 mmol) and NaOBz (0.288 g, 2.0 mmol) in 20 mL of EtOH and 5 mL of H_2O. Brown microcrystalline **11** precipitated (0.734 g, 53% yield). Anal. Calcd for $[Fe_2(BPA)_2O(OBz)_2](ClO_4)_2·H_2O$ ($C_{38}H_{38}Cl_2Fe_2N_6O_{14}$): C, 46.32; H, 3.89; N, 8.53. Found: C, 46.55; H, 3.92; N, 8.36.

Crystallographic Studies. Crystals of **1–3** suitable for X-ray diffraction studies were grown from acetone solutions that were slowly evaporated in an ethyl acetate bath. The crystals were all mounted on glass fibers and coated with a viscous hydrocarbon. All data were collected on an Enraf-Nonius CAD4 diffractometer with graphite-monochromated Mo Kα (λ = 0.71069 Å) radiation and the ω-scan method. All data were corrected for Lorentz and polarization effects. Some pertinent crystallographic details for **1–3** are collected in Table I, and further details are given in Table S1 of the supplementary material. Some specific details for each structure are discussed below. Each structure was solved with standard heavy-atom techniques. Hydrogen atoms were placed in calculated positions, assigned thermal parameters that were 20% greater than the B_{equiv} value of the atom to which they were bonded, and not refined. All ordered non-hydrogen atoms were refined anisotropically. Refinement was carried out with full-matrix least squares on F, with scattering factors from ref 27, and included anomalous dispersion terms.[28]

$[Fe_2(TPA)_2O(OBz)](ClO_4)_3·2H_2O$ (1). Two crystals of **1** were used for data collection. The first crystal abruptly decomposed or fell off of the mount after 4500 reflections, and a second crystal was used to finish data collection. The check reflections (three every 67 min) were used to scale the two data sets (R_{int} = 0.034). The data were corrected for absorption but not for secondary extinction. The structure solution proceeded normally. The perchlorate anions are likely disordered and have relatively large thermal parameters. Similarly, the bridging benzoate also has relatively large thermal parameters. Two oxygen atoms of water were located in the structure. Hydrogen atoms were not included for the water molecules. The final residual electron density in the difference map (maximum 0.88 e/Å^3) is located near the perchlorate anions.

$[Fe_2(TPA)_2O(OAc)](ClO_4)_3·H_2O(CH_3COCH_3)$ (2). A single crystal of **2** was used for data collection. Three typical reflections were checked every 67 min with negligible decay. The data were not corrected for absorption or extinction. The structure solution proceeded normally with the exception of the bridging acetate (which was disordered and modeled with two carbon atoms at half-occupancy for the CH_3 group), the perchlorate anions (two of which are clearly disordered and modeled with rigid groups in three orientations of occupancy 0.43, 0.42, and 0.15 for ClO_4 (**2**) and four orientations of occupancy 0.36, 0.28, 0.20, and 0.16 for ClO_4 (**3**)), and a disordered solvent molecule (modeled with four carbon atoms). In principle, the solvent molecule may be acetone or ethyl acetate. Although the structure was solved assuming that the solvent was half an ethyl acetate, subsequent elemental analyses were consistent with the formulation of a single acetone as opposed to half an ethyl acetate. Hydrogen atoms were omitted for the $-CH_3$ group of the acetate, a water molecule, and the disordered acetone. The final residual electron density in the difference map (maximum 1.17 e/Å^3) is located near the perchlorate anions and the disordered solvent.

$[Fe_2(TPA)_2O(O_2P\{OPh\}_2)](ClO_4)_3·(CH_3COCH_3)$ (3). Two crystals of **3** were used for data collection. The first crystal slowly decomposed (three test reflections were checked every 83 min) in the X-ray beam and then split off of the mount. The second crystal also decomposed, but lasted through data collection. The two data sets were linearly corrected for decomposition and combined (R_{int} = 0.085). Since two crystals were used for data collection, the data were not corrected for absorption, but were corrected for Lorentz and polarization effects. They were also corrected for secondary extinction. The structure solution proceeded normally in the space group $P\bar{1}$. The choice of $P\bar{1}$ is confirmed on the basis of packing considerations, a statistical analysis of intensity distribution, and the successful solution and refinement of the structure. The final residual electron density in the difference map (maximum 1.12 e/Å^3) is near the perchlorate anions, which are probably somewhat disordered.

Physical Methods. Visible spectra were recorded on a Hewlett-Packard 8541A diode array spectrometer. ^1H NMR spectra were recorded on an IBM AC 300 spectrometer at 300 MHz. Chemical shifts (ppm) were referenced to residual protic solvent peaks. Magnetic susceptibility data were recorded over a temperature range of 10–300 K at a measuring field of 2.0 kOe with an SHE Corp. VTS-50 superconducting SQUID susceptometer interfaced to an IBM 9000 computer system. Calibration and operating procedures have been reported elsewhere.[11,29]

Raman spectra were recorded on a computerized Jarrell–Ash spectrophotometer with an RCA C31034A photomultiplier tube and an Ortec Model 9302 amplifier–discriminator or on a Dilor Z24 spectrophotometer. Excitation sources were Spectra-Physics 164-05 (Ar) and 2025-11 (Kr) lasers. For measuring the scattering intensity, solid samples were mixed with a known amount of sodium sulfate and run in a spinning sample holder at room temperature with a 150° backscattering geometry. For isotope comparisons, samples were dissolved in dry acetonitrile (refluxed 24 h in the presence of CaH_2 and freshly distilled over molecular sieves) plus 2% (v/v) $H_2{}^{16}O$ or $H_2{}^{18}O$ (85 atom %, Monsanto or 95 atom %, Yeda). Samples, containing 2–5 mg of complex/mL of acetonitrile, were sealed in capillaries and examined at room temperature with a 90° scattering geometry. Raman frequencies were corrected with an indene standard.[30]

Infrared spectra were collected on a Perkin-Elmer 1800 FT-IR spectrophotometer. Solid samples were run as KBr pellets. For isotope comparisons the samples in acetonitrile + 2% water were dried under nitrogen on an NaCl plate and run in a sample compartment purged with dry air.

Results

Crystallographic Studies. X-ray diffraction studies have been conducted on complexes **1–3**. A preliminary report of the structures of **1** and **2** has appeared previously.[24] All three complexes have a (μ-oxo)diiron core that is additionally bridged by a three-atom O–X–O group (where X = C or P), and the two iron atoms of each complex have distinct coordination environments. Figure 1 shows an ORTEP plot for **3** with the atomic numbering scheme excluding the carbon atoms, while the numbering scheme for the carbon atoms is found in Figure S1 of the supplementary material. The atomic coordinates of the nonhydrogen atoms for **1–3** are listed in Tables A–C, respectively, of the supplementary material. Table II presents relevant distances

(25) Anderegg, G.; Wenk, F. *Helv. Chim. Acta* **1967**, *50*, 2330–2332.
(26) Gafford, B. G.; Holwerda, R. A. *Inorg. Chem.* **1989**, *28*, 60–66.
(27) Cromer, D. T.; Waber, J. T. *International Tables for X-ray Crystallography*; Kynoch Press: Birmingham, England, 1974; Vol. IV, Table 2.2 A.
(28) Cromer, D. T. *International Tables for X-ray Crystallography*; Kynoch Press: Birmingham, England, 1974; Vol. IV, Table 2.3.1.
(29) O'Connor, C. J. *Prog. Inorg. Chem.* **1979**, *29*, 204–283.
(30) Hendra, P. J.; Loader, E. J. *Chem. Ind.* **1968**, 718.

Table II. Relevant Distances and Angles for $[Fe_2(TPA)_2O(O_2X)](ClO_4)_3$ Complexes[a]

param	1	2	3
Fe1···Fe2	3.241 (1)	3.243 (1)	3.357 (3)
Fe1–O12–Fe2	129.7 (3)	129.2 (2)	138.1 (2)
Fe1–O12	1.804 (5)	1.800 (4)	1.815 (3)
Fe2–O12	1.776 (4)	1.790 (5)	1.779 (3)
Fe1–O1C	1.984 (5)	1.972 (6)	1.963 (3)
Fe2–O2C	2.046 (5)	2.038 (6)	2.045 (3)
Fe1–N1A	2.190 (6)	2.198 (7)	2.178 (4)
Fe1–N2A	2.132 (7)	2.128 (6)	2.122 (4)
Fe1–N3A	2.185 (6)	2.199 (6)	2.184 (4)
Fe1–N4A	2.115 (6)	2.125 (6)	2.130 (4)
Fe2–N1B	2.218 (6)	2.242 (6)	2.239 (4)
Fe2–N2B	2.131 (6)	2.133 (6)	2.127 (4)
Fe2–N3B	2.138 (6)	2.154 (6)	2.130 (4)
Fe2–N4B	2.118 (6)	2.105 (6)	2.121 (4)
O12–Fe1–N1A	92.3 (2)	95.4 (2)	95.5 (1)
O12–Fe1–N2A	92.7 (2)	94.1 (2)	94.9 (1)
O12–Fe1–N3A	170.6 (2)	173.0 (2)	173.5 (1)
O12–Fe1–N4A	95.9 (2)	93.5 (2)	94.3 (1)
O12–Fe1–O1C	101.1 (2)	101.5 (2)	100.3 (1)
N1A–Fe1–N2A	77.4 (2)	77.8 (2)	78.0 (2)
N1A–Fe1–N3A	78.6 (2)	78.4 (2)	78.1 (1)
N1A–Fe1–N4A	76.6 (2)	76.0 (2)	77.4 (2)
N1A–Fe1–O1C	166.0 (2)	162.8 (2)	164.2 (1)
N2A–Fe1–N3A	83.2 (2)	81.7 (2)	85.2 (1)
N2A–Fe1–N4A	152.9 (2)	153.3 (2)	154.4 (1)
N2A–Fe1–O1C	105.4 (3)	104.3 (2)	101.8 (2)
N3A–Fe1–N4A	84.3 (2)	87.9 (2)	83.0 (1)
N3A–Fe1–O1C	88.1 (2)	85.0 (2)	86.1 (1)
N4A–Fe1–O1C	98.0 (2)	99.2 (2)	100.0 (2)
O12–Fe2–N1B	175.4 (2)	176.2 (2)	178.0 (1)
O12–Fe2–N2B	101.9 (2)	102.7 (2)	104.3 (2)
O12–Fe2–N3B	96.7 (2)	98.1 (2)	99.0 (2)
O12–Fe2–N4B	105.2 (2)	104.2 (2)	102.8 (2)
O12–Fe2–O2C	98.8 (2)	100.0 (2)	98.3 (1)
N1B–Fe2N2B	76.4 (2)	77.6 (2)	76.2 (2)
N1B–Fe2–N3B	79.0 (2)	78.2 (2)	79.1 (2)
N1B–Fe2–N4B	76.3 (2)	75.4 (2)	76.6 (2)
N1B–Fe2–O2C	85.5 (2)	83.7 (2)	83.6 (1)
N2B–Fe2–N3B	88.4 (2)	82.4 (2)	88.5 (2)
N2B–Fe2–N4B	152.6 (2)	152.9 (2)	152.8 (1)
N2B–Fe2–O2C	89.0 (2)	89.5 (2)	91.1 (1)
N3B–Fe2–N4B	83.9 (2)	90.7 (2)	86.0 (2)
N3B–Fe2–O2C	164.5 (2)	161.4 (2)	162.3 (1)
N4B–Fe2–O2C	91.5 (2)	88.9 (2)	86.3 (1)

[a] All distances in angstroms. All angles in degrees. For atom labels, see Figure 1.

and angles, while Table III compares the salient structural parameters of **1–3** with those of related complexes. Figure 2 compares the averaged structural features of **1** and **2** with $[Fe_2O(OAc)_2(tpbn)]_2^{4+}$, a representative tribridged complex.[5] Compound **4** ($[Fe_2(HDP)_2O(OBz)]BPh_4$) is another dibridged complex of the μ-oxo–μ-carboxylato variety;[22] compounds **5–8** (**5**, $[Fe_2(Me_3tacn)_2O(OAc)_2](ClO_4)_2\cdot H_2O$;[3] **6**, $[Fe_2(HB(pz)_3)_2O(OAc)_2]\cdot 4CH_3CN$;[4] **7**, $[Fe_2(BBA)_2O(OBz)_2](ClO_4)_2\cdot 2EtOH\cdot 0.5Et_3NHClO_4$;[6] **8**, $[Fe_2O(OAc)_2Cl_2(bipy)_2]\cdot CH_3CN$)[10] are tribridged (μ-oxo)bis(μ-carboxylato)diiron(III) complexes; and compounds **9**, $[Fe_2(Me_3tacn)_2O(O_3P\{OPh\})_2]\cdot NaClO_4\cdot H_2O$,[9] and **10**, $[Fe_2(HB(pz)_3)_2O(O_2P\{OPh\}_2)_2]$,[8] are bis(μ-phosphato) analogues of **5** and **6**, respectively.

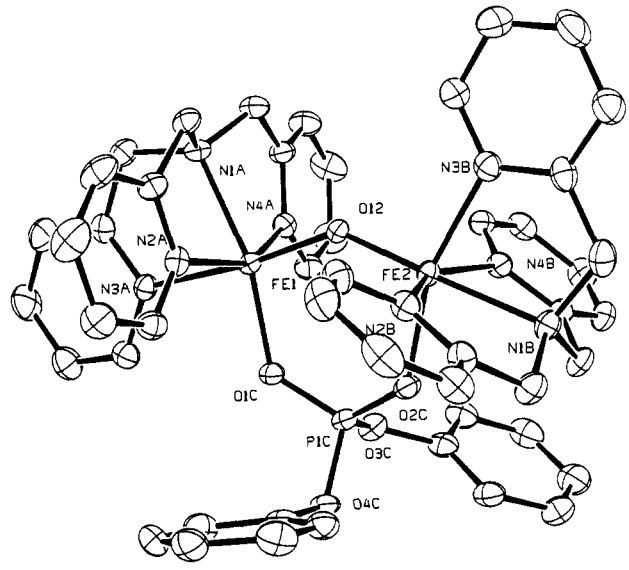

Figure 1. ORTEP drawing of $[Fe_2(TPA)_2O(O_2P\{OPh\}_2)]^{3+}$ showing a partial numbering scheme (carbon atoms are not labeled—a diagram of the ligand atom numbering scheme is in the supplementary material). The hydrogen atoms are omitted. The TPA ligand with "A" labels is bound to Fe1 and has N3A (a pyridine nitrogen) trans to the μ-oxo bridge, while the TPA ligand with "B" labels is bound to Fe2 and has N1B (a tertiary amine nitrogen) trans to the μ-oxo bridge.

A general feature of the dibridged species is that their structural parameters are similar but not identical with those of their tribridged counterparts. Thus, **1–4** have short $Fe–O_{oxo}$ bonds that fall into the 1.77–1.82-Å range found for the other (μ-oxo)diiron units, **5–10** (Table III). The single carboxylate bridge in **1** and **2** constrains the Fe···Fe distance to 3.24 Å and the $Fe–O_b–Fe$ angle to 129°. These values are comparable to those found for **4**, the other dibridged complex, but are somewhat larger than the respective values of 3.08–3.15 Å and 119–124° for the tribridged complexes **5–8**.

It is interesting to note that the core dimensions for the dibridged complexes more closely approximate those found for methemerythrin[2] and ribonucleotide reductase[31] than do the

Table III. Comparison of Relevant Distances and Angles for (μ-Oxo)diiron(III) Complexes[a]

feature[b]	1	2	3	4	5	6	7	8	9	10
Fe···Fe	3.241 (1)	3.243 (1)	3.357 (3)	3.218 (2)	3.12 (1)	3.1457 (6)	3.079 (2)	3.151 (1)	3.198 (3)	3.337 (1)
$Fe–O_b–Fe$	129.7 (3)	129.2 (2)	138.1 (2)	128.3 (3)	119.7 (1)	123.5 (1)	118.7 (3)	123.9 (2)	123.2 (3)	134.7 (3)
$Fe–O_b$	1.804 (5)	1.800 (4)	1.815 (3)	1.777 (6)	1.800 (3)	1.783 (2)	1.777 (5)	1.783 (4)	1.817 (5)	1.804 (5)
	1.776 (4)	1.790 (5)	1.779 (3)	1.799 (6)		1.787 (2)	1.802 (6)	1.787 (4)	1.818 (5)	1.812 (5)
Fe–N(3°)	2.190 (6)[c]	2.198 (7)[c]	2.178 (4)[c]	2.266 (7)[c]	2.198 (4)				2.242	
	2.218 (6)[d]	2.242 (6)[d]	2.239 (4)[d]	2.277 (9)[c]	2.268 (6)[c]				2.294[c]	
$Fe–O_{acido}$	2.046 (5)	2.038 (6)	2.045 (3)	2.059 (6)	2.034 (3)	2.044	2.036	2.080	1.983	2.045
	1.984 (5)[e]	1.972 (6)[e]	1.963 (3)[e]	2.082 (7)						
$Fe–N_{ar}$	2.124	2.123	2.125	2.166		2.151	2.112	2.150		2.130
	2.138 (6)[d]	2.154 (6)[d]	2.130 (4)[d]			2.177 (3)[d]		2.204 (5)[c]		2.210 (7)[c]
	2.185 (6)[c]	2.199 (6)[c]	2.184 (4)[c]			2.197 (3)[c]		2.212 (5)[c]		2.213 (6)[c]
ref	*f*	*f*	*f*	22	3b	4	6	10	9	8

[a] **1**, $[Fe_2(TPA)_2O(OBz)](ClO_4)_3\cdot 2H_2O$; **2**, $[Fe_2(TPA)_2O(OAc)](ClO_4)_3\cdot H_2O\cdot(CH_3COCH_3)$; **3**, $[Fe_2(TPA)_2O(O_2P\{OPh\}_2)](ClO_4)_3\cdot(CH_3COCH_3)$; **4**, $[Fe_2(HDP)_2O(OBz)]B(Ph)_4$; **5**, $[Fe_2(Me_3tacn)_2O(OAc)_2](ClO_4)_2\cdot H_2O$; **6**, $[Fe_2(HB(pz)_3)_2O(OAc)_2]$; **7**, $[Fe_2(BBA)_2O(OBz)_2](ClO_4)_2\cdot 2EtOH\cdot 0.5(Et_3NHClO_4)$; **8**, $[Fe_2O(OAc)_2Cl_2(bipy)_2]$; **9**, $[Fe_2(Me_3tacn)_2O(O_3P\{OPh\})_2]\cdot NaClO_4\cdot H_2O$; **10**, $[Fe_2(HB(pz)_3)_2O(O_2P\{OPh\}_2)_2]$. [b] O_b refers to the oxo bridge. N(3°) refers to the tertiary amine nitrogen. O_{acido} refers to the oxygen atoms of carboxylate or phosphate bridges. N_{ar} refers to aromatic nitrogen atoms. Those values without standard deviations are averages. [c] These atoms are trans to the oxo bridge. [d] This ligand is contained in the effective mirror plane defined by the Fe–O–Fe moeity. [e] This oxygen atom is trans to the tertiary amine. [f] This work.

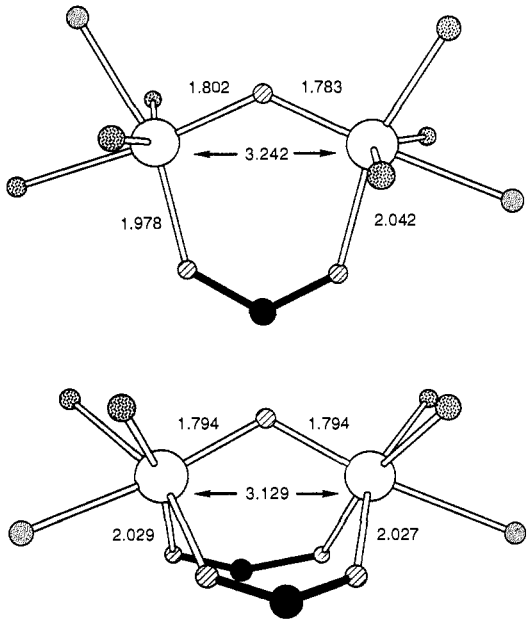

Figure 2. Comparison of the averaged core dimensions of $[Fe_2(TPA)_2O(OBz)]^{3+}$ and $[Fe_2(TPA)_2O(OAc)]^{3+}$ (top) with the core dimensions of $[Fe_2O(OAc)_2(tpbn)]_2^{4+}$ from ref 5 (bottom).

tribridged complexes. The tribridged complexes have Fe···Fe distances and Fe–O_b–Fe angles that are smaller than those found in the (μ-oxo)diiron(III) proteins. We initially speculated[15] that the smaller values for the tribridged Me_3tacn and $HB(pz)_3$ complexes **5** and **6** may be due to the small N_{cis}–Fe–N_{cis} angles required by the face-capping ligands, which results in the ligands on the opposite face having larger O–Fe–O angles and thus shorter Fe–Fe distances. Yet the N_{cis}–Fe–N_{cis} angles in the TPA complexes **1–3** are only slightly larger (average 85.5°) than those found in the $HB(pz)_3$ complexes (average 83.2°). Additionally, the similarity of the core dimensions of the tribridged **8** with bidentate bipy and monodentate chloride ligands to those of the other tribridged complexes discounts this argument, since the N_2Cl face of the bipy complex would not suffer the same constraints as the complexes of the tridentate ligands. Although the TPA ligand has the flexibility to provide nearly ideal trigonal geometry (as in $[Cu(TPA)Cl]^+$),[32] the N_{cis}–Fe–N_{cis} angles in **1–3** are the smallest for all TPA complexes reported to date.[26,33] Thus, it would appear that the Fe···Fe distances and the Fe–O–Fe angles found in **1** and **2** are a result of the (μ-oxo)(μ-carboxylato)diiron core rather than a feature of the tripodal ligands.

The conversion of a tribridged core to a dibridged one entails the ~45° rotation about the Fe–O_b vectors placing the bridging carboxylate in the Fe–O–Fe plane:

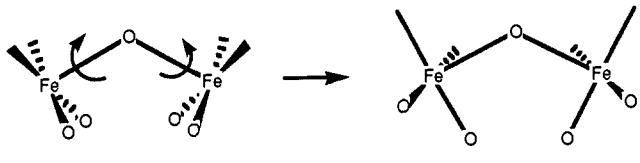

This operation is analogous to changing two face-sharing octahedra to two edge-sharing octahedra, which typically results in an increased metal–metal separation and an increase in the average angle at the bridging atom.[34-36]

The replacement of the carboxylates with diphenyl phosphate (to give **3**) engenders the expected changes in the core dimensions. Because of the larger bite of the phosphate ligand, the Fe···Fe separation and the Fe–O_b–Fe angle increase to 3.36 Å and 138°, respectively. None of the other Fe–ligand distances change significantly, including the Fe–O_{acido} distance relative to those of carboxylates **1** and **2**. Similar increases in core dimension are also observed for **9** and **10** relative to their acetate analogues, **5** and **6**. Yet in these complexes the other iron to ligand distances are changed. With the substitution of $O_2P\{OPh\}_2^-$ for OAc in **6** to yield **10**, the average Fe–O_b lengthens from 1.785 to 1.808 Å and the average Fe–N_{ar} decreases from 2.151 to 2.130 Å. The ligand parameters also have changed in **9** relative to **5**, but the situation is complicated by the concomitant increase of charge on the bridging ligand ($O_3P\{OPh\}^{2-}$). Thus, the average Fe–O_b lengthens, as does the average Fe–N3^0, but the average Fe–O_{acido} decreases. In keeping with the expected core enlargement of dibridged complexes relative to tribridged complexes, dibridged species **3** shows slightly larger core parameters than the tribridged cases (**9** and **10**).

The most unusual feature of the TPA complexes is the inequivalence of the two iron sites. The two TPA ligands in a given complex have two different orientations (Figure 1). The TPA ligand associated with Fe1 contains a pyridine ring trans to the oxo bridge, while the TPA ligand associated with Fe2 has the tertiary amine trans to the oxo bridge. As a result, in complexes **1–3**, the Fe–N_{py} bond trans to the oxo bridge (2.18–2.20 Å) is significantly longer than the other five (2.11–2.16 Å, average 2.13 Å). There is also a significant difference in the lengths of the two Fe–N tertiary amine bonds in the TPA complexes, with the tertiary amine bond trans to the oxo bridge (2.22–2.24 Å) significantly longer (2.18–2.20 Å) than that cis to the bridge. Such trans effects of oxo bridges have been noted previously.[3b,4,33a,b] The TPA complexes have an effective mirror plane of symmetry containing the Fe–O–Fe moiety. Thus, pyridine rings 2A and 4A are related by this mirror (the pyridine rings are labeled according to the label of the pyridine nitrogen atom of the ring), as are rings 2B and 4B. Ring 3A, the pyridine trans to the oxo bridge, is contained in the effective mirror plane, while ring 3B, which is also contained in the mirror plane, is cis to the oxo bridge. However, this plane does not interrelate the two iron sites. Previously investigated tribridged (μ-oxo)diiron complexes exhibit an effective 2-fold symmetry axis through the bridging oxide, which affords iron atoms with nearly identical coordination environments. The effective 2-fold axis is absent in the TPA complexes reported here, making them the first examples of (μ-oxo)(μ-carboxylato)diiron complexes containing distinct iron sites.

The carboxylato (or phosphato) group in **1–3** bridges unsymmetrically to the (μ-oxo)diiron unit as a result of the inequivalence of the iron sites. On Fe1 the XO_2 bridge is trans to the tertiary amine nitrogen, while on Fe2 it is trans to a pyridine nitrogen. Thus, the Fe1–O_{acido} bond (average 1.972 Å) is shorter than the Fe2–O_{acido} bond (average 2.042 Å). Similarly unsymmetric carboxylate bridges have been noted previously for **8** (average 2.150 and 2.010 Å) and $Me_4N[Fe_2(HXTA)(OAc)_2]$ (average 1.970 and 2.050 Å)[12] as a result of different trans ligands, but not for complexes **4–7**. The rest of the structural parameters associated with the ligands and the perchlorates in **1–3** are all as expected.

Physical Properties. The dibridged complexes closely resemble the tribridged complexes with respect to their electronic,

(31) (a) Scarrow, R. C.; Maroney, M. J.; Palmer, S. M.; Que, L., Jr.; Salowe, S. P.; Stubbe, J. *J. Am. Chem. Soc.* **1986**, *108*, 6832–6834. (b) Bunker, G.; Petersson, L.; Sjöberg, B.-M.; Sahlin, M.; Chance, M.; Chance, B.; Enrenberg, A. *Biochemistry* **1987**, *26*, 4708–4716. Also see: footnote 64 in reference 15.

(32) Karlin, K. D.; Hayes, J. C.; Juen, S.; Hutchinson, J. P.; Zubieta, J. *Inorg. Chem.* **1982**, *21*, 4106–4108.

(33) (a) Gafford, B. G.; Holwerda, R. A.; Schugar, H. J.; Potenza, J. A. *Inorg. Chem.* **1988**, *27*, 1126–1128. (b) Towle, D. K.; Botsford, C. A.; Hodgson, D. J. *Inorg. Chim. Acta* **1988**, *141*, 167–168. (c) Hodgson, D. J.; Zietlow, M. H.; Pedersen, E.; Toftlund, H. *Inorg. Chim. Acta* **1988**, *149*, 111–117.

(34) Compare $[Fe^{II}_2(OR)_3]$ with $[Fe^{II}_2(OR')_2]$ in (a) and (b), respectively. (a) Shibata, S.; Onuma, S.; Iwase, A.; Inoue, H. *Inorg. Chim. Acta* **1977**, *25*, 33–39. (b) Snyder, B. S.; Patterson, G. S.; Abrahamson, A. J.; Holm, R. H. *J. Am. Chem. Soc.* **1989**, *111*, 5214.

(35) Compare $[Co^{II}_2(OR)_3]$ with $[Co^{II}_2(OR)_2]$ in Cotton, F. A.; Elder, R. C. *Inorg. Chem.* **1965**, *4*, 1145–1151.

(36) Compare $[Cu^{II}_2Cl_3]$ with $[Cu^{II}_2Cl_2]$ in (a) and (b), respectively. (a) Schuetler, A. W.; Jacobson, R. A.; Rundle, R. E. *Inorg. Chem.* **1966**, *5*, 277–280. (b) Willet, R. D.; Dwiggens, C.; Kruh, R. F.; Rundle, R. E. *J. Chem. Phys.* **1963**, *38*, 2429–2436.

Table IV. Magnetic, Mössbauer, and Electronic Spectroscopic Properties of (μ-Oxo)diiron(III) Complexes[a]

	1	2	3	5	6	7	9	10	11
				Electronic Spectra					
λ_{max} (ϵ)[b]	246 (34)	248 (25)	252 (28)		262 (3.4)				
	328 (12)	332 (10)	322 (14)	345 (10.5)	339 (4.6)		332 (7.0)	320 (5.8)	324 (8.3)
	368 (sh)	366 (sh)	360 (7.7)		358 (sh)	355 (4.0)	355 (sh)	365 (5.2)	360 (sh)
				424 (0.96)			416 (1.4)		414 (sh)
	460 (1.2)	458 (1.2)	446 (0.85)	472 (1.4)	457 (0.51)	485 (0.31)	482 (0.55)	478 (0.26)	450 (1.3)
	492 (1.0)	492 (1.0)	480 (0.66)		492 (0.46)		495 (sh)		498 (0.89)
	504 (0.98)	504 (0.94)	496 (0.56)						
	534 (sh)	534 (sh)	518 (sh)	513 (1.1)	528 (sh)	525 (0.11)	523 (0.27)		536 (sh)
				549 (sh)		560 (0.05)			
	700 (0.16)	700 (0.14)	638 (0.15)	729 (0.14)	695 (0.07)	620 (0.05)	627 (0.19)	624 (0.07)	704 (0.15)
				1031 (0.007)	995 (0.004)				
				Mössbauer Spectra					
δ (mm/s)	0.45	0.45		0.47 (3)	0.52 (3)				
ΔE_Q (mm/s)	1.52	1.45		1.50 (5)	1.60 (5)				
				Magnetic Properties					
$-J$ (cm^{-1})	118.6	114.3	101.1	119	121.3	117	98	98	118.6
TIP (cgsμ/mol)	0.000 03	0.000 17	0.000 29						0.000 06
p (mol %)	0.045	0.44	0.084						0.019
g	2.06	2.03	2.04						2.04
ref	24,c	24,c	24,c	3b	4	6	9	8	c

[a] Complexes as described in Table VI. [b] λ_{max} in nm (ϵ in mM^{-1} cm^{-1}). [c] This work.

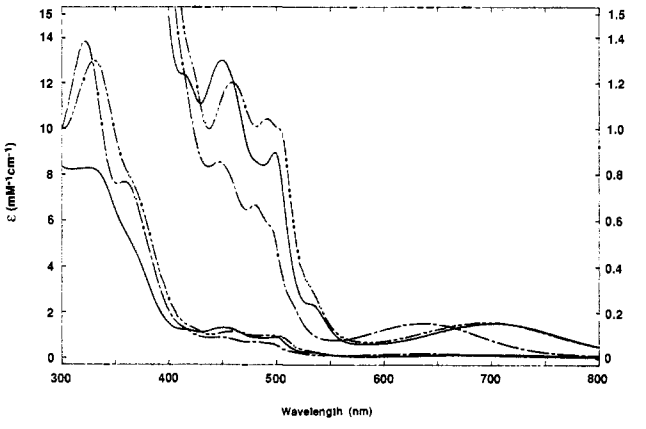

Figure 3. Electronic spectra of $[Fe_2(BPA)_2O(OBz)_2]^{2+}$ (—), $[Fe_2(TPA)_2O(OBz)]^{3+}$ (–··–), and $[Fe_2(TPA)_2O(O_2P\{OPh\}_2)]^{3+}$ (–·–) all in CH_3CN. Upper spectra correspond to axis labels to the right. Data are compared with other (μ-oxo)diiron(III) complexes in Table IV.

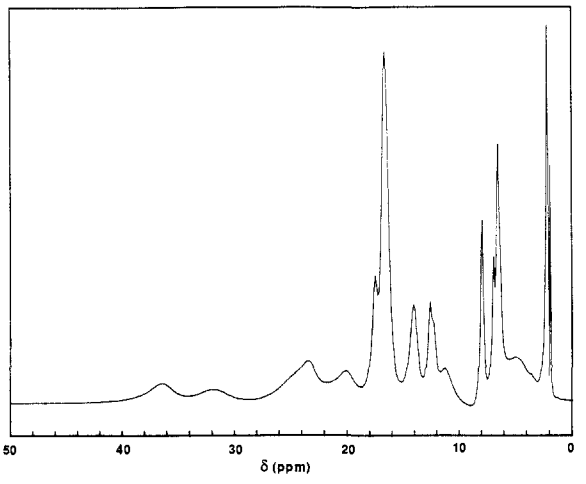

Figure 4. ^1H NMR spectrum of $[Fe_2(TPA)_2O(OAc)]^{3+}$ in CD_3CN.

Mössbauer, and magnetic properties (Table IV). The UV–vis spectra of **1** and **3** are compared with that of $[Fe_2(BPA)_2O(OBz)_2]^{2+}$ (**11**) in Figure 3. All exhibit similar features despite variations in the bridging components. **11** is representative of the (μ-oxo)bis(μ-carboxylato)diiron(III) family in having a feature near 330 nm, three features from 400 to 500 nm, a shoulder near 525 nm, and a broad band near 700 nm. The spectrum of **1** is very similar to that of **11**, while that of **3** is somewhat blue shifted. The differences between **1** and **3** may reflect the larger bite of the phosphate ligand and its affinity for Fe(III). Similar differences are observed for **9**[9] and **10**[8] relative to **5** and **6**. It is clear, however, that the observed visible spectral features are derived from the bent (μ-oxo)diiron(III) unit.[13,37] More systematic studies of the effects of changing the Fe–O–Fe angle and varying the charge of the bridging ligand are in progress.

The Mössbauer spectra of **1** and **2** each consist of a single quadrupole doublet with an isomer shift (δ, 0.45 mm/s) characteristic of a high-spin ferric center and a large quadrupole splitting (ΔE_Q, 1.52 and 1.45 mm/s, respectively) due to the presence of the oxo bridge.[24] For comparison, the ΔE_Q values for **5**, **6**, and **8** are 1.50, 1.60, and 1.80 mm/s, respectively. These parameters thus appear typical of complexes with (μ-oxo)diiron(III) cores irrespective of the number of carboxylate bridges or the equivalence of the ligand set on each iron atom.

Variable-temperature magnetic susceptibility measurements were made on **1–3** and **11**. The data can be found in Figures S2–S5 (supplementary material), while the fits of the data to the model of an isolated Heisenberg dimer of $S = {}^5/_2$ ions with the Hamiltonian $\mathcal{H} = -2JS_1 \cdot S_2$ are summarized in Table IV. It is clear that the strength of the antiferromagnetic coupling between the iron centers in a (μ-oxo)diiron(III) unit is not significantly affected by these differences in the Fe–O–Fe angle nor by the presence of one or two carboxylate bridges: $-J = 114–132$ cm^{-1} for **1**, **2**, **11**, and all of the structurally characterized (μ-oxo)bis(μ-carboxylato)diiron(III) complexes reported thus far.

The substitution of carboxylate with phosphate, however, weakens the antiferromagnetic interaction in **3** to $-J = 101$ cm^{-1}. Similarly, the $-J$ values for complexes **9** and **10** both decrease to 98 cm^{-1} when the carboxylate is changed to a phosphate. The phosphate substitution in the tribridged complexes results in a slight lengthening of the Fe–O_b bonds, which weakens the coupling interaction, as first pointed out by Gorun and Lippard.[38] However, similar bond lengthening is not observed on going from **2** to **3**.

Thus far, the dibridged complexes behave rather similarly to their tribridged analogues with respect to their electronic and

(37) Reem, R. C.; McCormick, J. M.; Richardson, D. E.; Devlin, F. J.; Stephens, P. J.; Musselman, R. L.; Solomon, E. I. *J. Am. Chem. Soc.* **1989**, *111*, 4688–4704.

(38) Gorun, S. M.; Lippard, S. J. *Recl. Trav. Chim. Pays-Bas* **1987**, *106*, 417.

Table V. ^{1}H NMR Parameters of TPA Complexes

1	2[a]	3	int[b]	assignment
37	36 (1.4)	42	2	*o*-pyr or CH_2
32	31 (1.2)	34	1	*o*-pyr or CH_2
23	23 (1.1)	26	2	*o*-pyr or CH_2
20	20 (nd)	22	1	*o*-pyr or CH_2
17.4	17.4 (5.3)	18.8	1	*m*-pyr
16.6	16.5 (5.2)	17.9	8	*m*-pyr
12.7	12.6 (6.9)[c]	13.9	1	*m*-pyr
12.3	12.3 (6.9)[c]	13.2	1	*m*-pyr
11	11.2 (nd)	12.4	1	*m*-pyr
8.0	7.9 (14.1)	8.0	2	*p*-pyr
6.9	6.9 (22.2)	6.9	1	*p*-pyr
6.5	6.5 (14.8)[c]	6.5	3 (2)[d]	*p*-pyr
	6.4 (14.8)[c]	6.2	1	*p*-pyr
	14.0 (2.2)		3	$OAcCH_3$
9.15				*m*-OBz
6.67				*p*-OBz
		7.4	10	Ph of $O_2P\{OPh\}_2^-$

[a] Figures in parentheses are relaxation times in milliseconds. [b] Relative intensity. [c] These two peaks are too close to measure separate relaxation times. [d] 1 has a relative intensity of 3; 2 and 3 have relative intensities of 2.

Mössbauer spectra and magnetism. These properties appear to be insensitive to the number of carboxylate bridges and, more importantly, the inequivalence of the iron sites.

^{1}H NMR Spectra. ^{1}H NMR spectroscopy was performed in order to confirm that the solid-state structure determined by X-ray crystallography persists in solution; namely, that complexes **1–3** contain two spectroscopically distinct iron sites. Figure 4 shows the ^{1}H NMR spectrum of **2**, and the chemical shifts for the three complexes are collected in Table V along with our proposed assignments. These assignments are based in part on comparisons with other TPA complexes (results to be published) and T_1 measurements for **2**.

All of the NMR features appear within 0–40 ppm, indicative of relatively strong antiferromagnetic coupling between the iron sites. Comparison of the ^{1}H NMR spectra of **1** and **2** suggests that the peaks at 9.15 and 6.67 ppm for **1** arise from the benzoate ring protons, while the peak at 14.0 ppm in the spectrum for **2** is the acetate CH_3. Similar comparisons suggest that the broad peak at 7.4 ppm in the spectrum of **3** arises from the ring protons of $O_2P\{OPh\}_2^-$. Comparison of the ^{1}H NMR spectrum of **1** with those of the 4-chlorobenzoate and 3,5-dichlorobenzoate analogues allows the assignment of the 9.15 ppm peak to the meta protons and the 6.67 ppm peak to the para protons.

The remaining peaks of the ^{1}H NMR spectra of **1–3** are easily separable into three groups in the following ranges: 6–8, 11–19, and 20–40 ppm, corresponding to the para protons of the pyridine rings, the meta protons of the pyridine rings, and a combination of the pyridine ortho and CH_2 protons, respectively. These assignments are made as follows. The peaks at 6–8 ppm are the sharpest and have the longest T_1's, indicating that they are the furthest removed (most distant) from the iron centers. They also exhibit the smallest paramagnetic shift. These observations are all consistent with their assignment as the para protons of the pyridine rings. They exhibit a relative intensity of 2:1:3 in compound **1** and 2:1:2:1 in compounds **2** and **3**. As discussed previously (see structure section), in the solid state, **1–3** contain distinct iron sites and distinct TPA orientations, suggesting that each TPA ligand would have a different 2:1 pattern. That is, two of the pyridines in each TPA ligand are in distinctly different environments from the third. This leads to the pattern observed for these para protons. Thus, the para protons having relative intensity of 1 are associated with TPA rings 3A and 3B (associated with the corresponding N atoms in Figure 1).

The ortho and CH_2 region (20–40 ppm) contains four peaks in two groups of relative intensity 2:1 and 2:1. These peaks are the broadest in the spectrum and have the shortest T_1's as expected for the ortho protons and the CH_2 protons, which are the closest to the Fe centers. While we are unable to definitively assign these resonances either to ortho or CH_2 protons[39] or to Fe1 or Fe2 at this time,[40] the appearance of two groupings of protons each with a 2:1 pattern suggests that there are two distinct orientations of TPA in the complexes in solution.

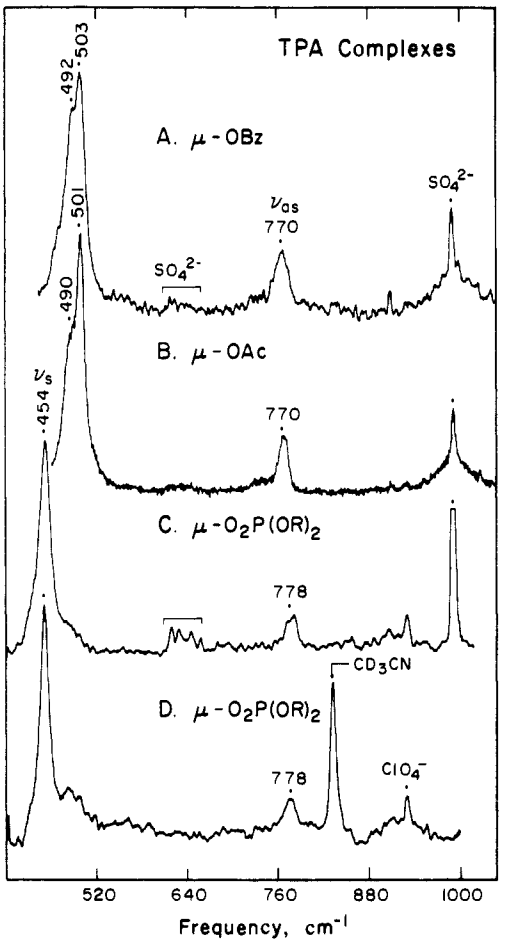

Figure 5. Resonance Raman spectra of TPA complexes: (A) solid **1** with 3× Na_2SO_4 (by weight); (B) solid **2** with 3× Na_2SO_4; (C) solid **3** with 3× Na_2SO_4; (D) **3** but dissolved in CD_3CN. Spectra in A and B obtained with 413.1-nm excitation, 40 mW, at a scan rate of 1 cm^{-1} s^{-1}, resolution 6 cm^{-1}, six scans. Spectra C and D collected under similar conditions but with 457.9-nm excitation, 30 mW.

The meta region (10–18 ppm) exhibits a relatively complex pattern of intensities (1:8:1:1:1).[41] It is easy to imagine that the peak of intensity 8 (at 16.6 ppm) arises from the meta protons of rings 2A, 4A, 2B, and 4B. These are all removed from the Fe–O_b–Fe plane. The remaining four peaks must then arise from the pyridine rings 3A and 3B, which are virtually coplanar with the Fe–O_b–Fe moiety. Of the meta protons of rings 3A and 3B, the proton bound to C7B is the closest to both iron atoms, is expected to give rise to the broadest signal, and is thus suggested to be assignable to the peak at 11 ppm, which is the broadest in this region.[42] The rest are comparably distant (8.1, 8.1, 8.4 Å)

(39) It is possible that some of the protons may be close enough to the iron centers to be broadened beyond detection—the ortho protons are all 3.2–3.3 Å from the iron(III) centers while four of the CH_2 protons are 3.2–3.3 Å from the iron(III) centers and the remaining eight protons are 3.7–4.0 Å away.

(40) The CH_2's about Fe1 are expected to be more distinct than those about Fe2. The CH_2 groups of each site are roughly equivalent in terms of distance from the Fe of their site, and this is the dominant effect. Additionally the three CH_2's about Fe2 are all nearly equidistant from Fe1 (7.0 Å for C17B, 6.2 Å for the others); however, the three CH_2's about Fe1 have significantly different distances to Fe2, C17A being further (6.7 Å) than C16A and C18A (5.1 Å). Thus, we suggest that the broadest, most paramagnetically shifted features at 37 and 32 ppm may arise from the protons of C16A and C18A for the former peak and of C17A for the latter.

(41) Alternatively, the pattern of intensities may be 1:9:1:1:1—integration of these peaks is difficult due to their breadth and overlapping nature.

(42) Another possibility is that this peak may arise from the CH_2 protons—it is considerably broader than the other meta protons.

Table VI. Vibrational Characteristics of (μ-Oxo)diiron(III) Complexes

complex	Fe–O–Fe stretch[a] $\nu_s(\Delta^{18}O)$	Fe–O–Fe stretch[a] $\nu_{as}(\Delta^{18}O)$	intensity ratio[b] I_s/I_{992}	intensity ratio[b] I_{as}/I_s
1 $[Fe_2(TPA)_2O(OBz)]^{3+}$	497[c] (17)	772 (37)	>160[d]	0.33[e]
2 $[Fe_2(TPA)_2O(OAc)]^{3+}$	449[c]	770 (38)	>140[d]	>0.22[d]
3 $[Fe_2(TPA)_2O(O_2P\{OR\}_2)]^{3+}$	454	778	230	0.18
4 $[Fe_2(HDP)_2O(OBz)]^{+}$	494 (17)	763	5	<0.04
5a $[Fe_2(tacn)_2O(OAc)_2]^{2+}$	540 (17)	749 (33)	35	<0.04
6 $[Fe_2(HB(pz)_3)_2O(OAc)_2]$	528 (17)	751 (30)	320	<0.04
7 $[Fe_2(BBA)_2O(OBz)_2]$	537	745 (45)	75	0.08
12 $[Fe_2(tmip)_2O(OPr)_2]^{2+}$	533	749	380	<0.04
13 $[Fe_2(tpbn)O(OAc)_2]_2^{4+}$	525	727	90	0.09
methemerythrin (N_3^-)	507 (14)	768 (35)	290	0.27
ribonucleotide reductase	493 (13)	756 (25)	>205[f]	0.20[e]

[a] Frequencies (cm^{-1}) shift to lower energy with μ-^{18}O. ν_s(Fe–O–Fe) from resonance Raman spectra of dibridged complexes in acetonitrile, tribridged complexes as solids, and protein samples in aqueous solution at 5 °C. ν_{as}(Fe–O–Fe) from IR spectra for tribridged and HDP complexes and from Raman spectra for TPA complexes and proteins. Sources of data: **5a**, ref 43; **6**, ref 4; **7**, ref 45; **12**, ref 13; proteins, ref 13. [b] I_s/I_{992} from the molar intensity (peak area/concentration) of ν_s(Fe–O–Fe) divided by the molar intensity of $\nu_1(SO_4^{2-})$ at 992 cm^{-1}. I_{as}/I_s calculated from peak area of ν_{as}(Fe–O–Fe) relative to ν_s(Fe–O–Fe). Excitation at 406.7 or 413.1 nm. Values for tribridged complexes and proteins.[13] [c] Midpoint of Fermi resonance doublet. [d] Based on area of higher energy Fermi resonance peak. [e] Calculated from spectrum of ^{18}O complex. [f] Minimum value owing to photosensitivity, based on two Fe–O–Fe units per metRRB2.[48]

and are difficult to assign. But again the dissimilar nature of the two sites is reflected by the NMR data.

In general, the shifts observed for **3** are slightly larger than the corresponding shifts for **1** and **2**. This pattern is to be expected, as the iron centers in **3** are less strongly coupled than those in **1** and **2** and thus should exert a larger paramagnetic effect.

The acetate CH_3 shift in **2** observed at 14.0 ppm can be compared to those of other complexes (**5**, **6**, $[Fe_2(BBA)_2O(OAc)_2](ClO_4)_2$,[6] and $[Fe_4O_2(5,6\text{-}Me_2HPTB)(OAc)_2](ClO_4)_4$[11]), which have acetate CH_3 shifts ranging from 9.8 to 10.9 ppm. Although the larger shift may at first glance be ascribed to weaker antiferromagnetic coupling in **2** relative to the complexes, it is clear that all these complexes exhibit very similar antiferromagnetic coupling ($J \sim -120$ cm^{-1}). Further studies are required to rationalize the "anomalous shift" observed in **2**.

Resonance Raman Spectra. The resonance Raman behavior of dibridged complexes **1**–**4** was investigated in order to determine the effects of the single carboxylate bridge and the inequivalence of the iron sites on the Fe–O–Fe vibrations. The Raman spectra of the TPA complexes (Figure 5) are typical of oxo-bridged species in that the dominant feature is the symmetric stretching mode, ν_s(Fe–O–Fe), at ~500 cm^{-1} in **1** and **2** and 454 cm^{-1} in **3**. The lower frequencies of this mode in the phosphate complex are consistent with the larger Fe–O–Fe angle found for this complex.[13] The only other prominent features in these spectra are the asymmetric stretch of the Fe–O–Fe moiety at 770–787 cm^{-1} and the broad band underlying $\nu_1(SO_4^{2-})$ at ~994 cm^{-1} that corresponds to the first overtone of the symmetric stretch.

The Fe–O–Fe vibrational modes can be more definitively identified by their shift to lower energy upon substitution of the μ-oxo group with ^{18}O. When μ-benzoato complex **1** is prepared in acetonitrile containing 2% $H_2{}^{18}O$, the 772-cm^{-1} peak shifts by 37 cm^{-1}, as expected for the ν_{as}(Fe–O–Fe) mode (Table VI). More surprisingly, the features at 491 and 503 cm^{-1} drop equally in intensity, and a single new peak appears at 480 cm^{-1}. It is likely that the two features in the spectrum of the ^{16}O sample represent a Fermi resonance doublet arising from the overlap of the ν_s(Fe–O–Fe) mode with a combination or overtone band at the same frequency. Hence, the ν_s(Fe–O–Fe) fundamental would be at 497 cm^{-1}, the center of the doublet. Use of the secular equation for calculating the Fe–O–Fe angle from ^{16}O and ^{18}O vibrational frequencies[44] yields a value of 124°, which is in reasonable agreement with the crystallographically determined angle of 130° (Tables II and III). The correspondence of the broad feature at 995 cm^{-1} to $2\nu_s$ provides additional support for the assignment of the fundamental at 497 cm^{-1}. The μ-acetato complex **2** shows the same type of Fermi resonance behavior, with an ~17-cm^{-1} shift in ^{18}O, but the new peak at ~480 cm^{-1} is broadened and difficult to quantitate. For comparison, dibridged μ-benzoato HDP complex **4** exhibits ν_s at ~494 cm^{-1}, which also shifts to 17 cm^{-1} upon ^{18}O substitution.

Previous studies have shown that the symmetric Fe–O–Fe mode is strongly enhanced in the proteins hemerythrin and ribonucleotide reductase with a molar intensity (I_s) relative to ν_1 of sulfate of greater than 200.[13] In contrast, the majority of the monobridged and tribridged Fe–O–Fe model complexes have relative intensities in the 10–100 range with near-UV excitation.[13] The only model complexes that fall within the hemerythrin range are triply bridged species with unsaturated nitrogen ligands such as imidazole or pyrazole cis and trans to the μ-oxo group.[13] Thus, complexes **6** and **12** with all terminal pyrazole or imidazole ligands exhibit I_s/I_{992} ratios of 320 and 380, respectively. Complex **5a** with only aliphatic amine ligands on the terminal faces has a ratio of 35; complexes with aromatic nitrogen ligands only cis to the oxo bridge such as **7** and **13** have slightly higher values (Table VI). The dibridged complexes exhibit the same type of behavior. HDP complex **4**, which has pyridines only cis to the μ-oxo group, has the expected low I_s/I_{992} value (5 with 403-nm excitation and 70 with 360-nm excitation), while TPA complexes **1**–**3**, with only one pyridine in the trans position and the remaining pyridines cis to the oxo bridge, have relative intensities of 140–230 (Table VI). The 140–160 values represent lower estimates because the intensity of the ν_s(Fe–O–Fe) mode in the Fermi doublet could be greater than that of the 502-cm^{-1} peak used in the calculation. These results suggest that doubly bridged diiron(III) centers are capable of showing the same extent of resonance enhancement of the ν_s(Fe–O–Fe) mode as is observed in hemerythrin and ribonucleotide reductase.

A final feature of interest is the asymmetric stretch of the Fe–O–Fe moiety that generally has a much smaller Raman intensity than the symmetric stretch. Typical values for I_{as}/I_s are less than 0.1, and this is borne out by the tribridged complexes **5a**, **6**, **7**, **12**, and **13**, as well as the dibridged HDP complex **4**, which all have effective 2-fold symmetry about the oxo bridge (Table VI). This intensity ratio can be markedly enhanced by asymmetry as is the case for the $[(N5)FeOFeCl_3]^+$ complex[45] where ν_{as}(Fe–O–Fe) is the dominant feature in the Raman spectrum and I_{as}/I_s has become greater than 4. The inequivalence in the coordination environments of the two iron atoms in TPA complexes **1**–**3** is sufficient to produce enhanced intensities for ν_{as} (Figure 5) and I_{as}/I_s values of 0.18–0.33 (Table VI). The fact that the relative peak heights for ν_{as} and ν_s are unaltered between the solid state and acetonitrile solution (Figure 5C,D) provides additional evidence for the continued asymmetry of these complexes in solution. The intensity ratios for the TPA complexes are reminiscent of the 0.20–0.27 range observed for the proteins (Table VI). In the case of hemerythrin, asymmetry is imposed on its dinuclear iron site by exogenous ligands binding to only one of the two iron atoms.[2]

Discussion

We have synthesized and structurally characterized a series of (μ-oxo)diiron(III) complexes that are additionally O,O′-bridged with a carboxylate or a phosphate ligand using the tetradentate tripodal ligand TPA. The dimensions of the (μ-oxo)(μ-carboxylato)diiron(III) core (Fe–μ–O) = 1.79 Å; Fe···Fe = 3.24; ∠Fe–O–Fe = 129°) compare well with those of the (μ-oxo)bis(μ-carboxylato)diiron(III) core found in a variety of complexes, although the Fe···Fe distance and the Fe–O–Fe angle are con-

(43) Spool, A.; Williams, I. D.; Lippard, S. J. *Inorg. Chem.* **1985**, *24*, 2156–2162.

(44) Wing, R. M.; Callahan, K. P. *Inorg. Chem.* **1969**, *8*, 871.

(45) Gomez-Romero, P.; Witten, E. H.; Reiff, W. M.; Backes, G.; Sanders-Loehr, J.; Jameson, G. B. *J. Am. Chem. Soc.* **1989**, *111*, 9039–9047.

sistently larger for the dibridged complexes, as to be expected on the basis of the analogy to conversion of two face-sharing octahedra to two edge-sharing octahedra (see above). Complexes with the dibridged core also exhibit electronic spectral features, Mössbauer parameters, and magnetic properties similar to those of analogous complexes with the tribridged core. This similarity suggests that the spectral and magnetic properties are dominated by the oxo bridge and only weakly modulated by the bridging carboxylates/phosphates.

The unique structural feature of the TPA complexes is the inequivalence of the two iron sites. We have not established what gives rise to the inequivalence, but it is clear that crystal packing does not play a major role since the inequivalence persists in solution on the basis of the NMR and Raman spectra of the complexes. We suspect that unfavorable interligand steric interactions prevent the formation of a symmetric structure analogous to that found in the corresponding HDP complex, **4**. Molecular modeling studies suggest that, for the symmetric structure wherein the iron environment on Fe2 is duplicated on Fe1, an unfavorable steric interaction would occur between the ortho protons on pyridines 2B and 4B of one iron center and the corresponding protons of the other iron center, making this configuration energetically unfavorable. Such a structure places both weakly coordinating tertiary amine nitrogen atoms trans to the oxo bridge and would presumably be the configuration preferred by the (μ-oxo)diiron core from an electronic standpoint, since this configuration is found in the structures of **4**, **7**, and other tribridged complexes with combinations of tertiary amine and aromatic nitrogen ligands.[5] A similar steric argument has been put forth to rationalize the preferred trans configuration of the aliphatic nitrogen atoms relative to the Cr_2O_2 core in $[Cr_2(OH)_2(TPA)_2]^{4+}$, which is analogous to the configuration found for the TPA complexes discussed here.[33c]

The inequivalence of the iron environments in **1–3** has no apparent significant effect on the electronic spectral, Mössbauer, and magnetic properties of the complexes as judged from comparisons with complexes with equivalent iron sites. However, the inequivalence is strongly reflected in the NMR and resonance Raman properties of the complexes. In the NMR spectra, the relative integrations and the multiplicity of peaks associated with a particular type of proton emphasize the absence of 2-fold symmetry in the complexes. In the resonance Raman spectra, the ν_s(Fe–O–Fe) and the ν_{as}(Fe–O–Fe) features associated with the unsymmetric dibridged core have intensities that differ significantly from those found in the complexes with 2-fold symmetry, but model well features found in the protein spectra.

Sanders-Loehr et al. have undertaken an investigation of the factors that affect the intensities of these vibrations in a series of (μ-oxo)diiron(III) complexes.[13] In this series, the intensity of the ν_s(Fe–O–Fe) is enhanced by the presence of multiple bridging groups and the presence of aromatic nitrogen ligands cis and, more importantly, trans to the oxo bridge. The dibridged complexes in this study follow these general trends. **4**, with pyridines cis to the oxo bridge, has a maximal I_s/I_{992} = 70 (with 360-nm excitation), and **1–3**, each with an additional pyridine trans to the oxo bridge, show I_s/I_{992} = 140–230. The fact that the values found for **1–3** are about half of those found for the $HB(pz)_3$ and tmip complexes (**6** and **12**, respectively) is consistent with the presence of only one aromatic ligand trans to the oxo bridge in **1–3**, compared to two in the latter complexes.

The inequivalence of the iron sites in **1–3** also affects the intensity of ν_{as}(Fe–O–Fe). This vibration generally occurs as a strong feature in the infrared spectrum and as a weak or nonobservable feature in the Raman spectrum. For **4** and other complexes with equivalent iron sites, the I_{as}/I_s ratio is no greater than 0.09 and, in many cases, <0.04. When the two iron sites become dramatically inequivalent, as in $[(N5)FeOFeCl_3]^+$,[45] the I_{as}/I_s ratio can be as large as 4.2. (It should be noted that the value is due not only to the enhancement of ν_{as} but also to the lower intensity of ν_s in this complex.) In the cases of **1–3**, where the inequivalence in the iron sites is not as pronounced as in $[(N5)FeOFeCl_3]^+$, the I_{as}/I_s ratio is 0.18–0.33.

Insight into the coordination environment of the diiron site in the ribonucleotide reductase from *E. coli* can be gleaned from a comparison of its properties with those of methemerythrin and the model complexes. That the enzyme has a (μ-oxo)diiron core has been established by a combination of Mössubaer, magnetic susceptibility, resonance Raman, and EXAFS measurements.[14,15] The presence of additional bridges to the diiron core is indicated by the Fe···Fe distance of 3.22 Å determined by EXAFS[31] and the similarity of its electronic spectral features to those of methemerythrin and the di- and tribridged model complexes.[4,15] Although a (μ-oxo)bis(μ-carboxylato)diiron core has been proposed for this site,[4,15] the physical and structural properties of the diiron site are also consistent with a dibridged diiron core structure.

The possible ligand environments for the diiron site in ribonucleotide reductase are further constrained by the Raman data. Ribonucleotide reductase is found to exhibit I_s/I_{992} and I_{as}/I_s ratios of >205 and 0.20, respectively. The I_s/I_{992} value is somewhat smaller than those of methemerythrin and the synthetic complexes with aromatic nitrogen ligands both cis and trans to the oxo bridge (i.e., the $HB(pz)_3$ and tmip complexes) but comparable to that of **3**, which has only one pyridine trans and several pyridines cis to the oxo bridge. The ribonucleotide reductase value can be interpreted in one of two ways: (a) that the diiron center in the enzyme has a coordination environment similar to that found in **1–3** with one His trans and other His ligands cis to the oxo bridge, or (b) that there is one His on each iron atom trans to the oxo bridge with no other His ligands to the diiron core. Independent evidence for histidine ligation has been obtained from NMR[46] and EXAFS[31b] studies, and the latter suggest that there may be less than 1.5 His/iron atom in support of interpretation b.

The I_{as}/I_s ratio of 0.20 for ribonucleotide reductase is comparable to ratios found for **1–3** and the methemerythrin–X complexes,[13] suggesting an iron site inequivalence similar to those observed for the other complexes. The I_{as}/I_s ratio thus implicates a diiron core that is inherently unsymmetric, in agreement with the earlier Mössbauer observation of two iron centers having distinct quadrupole splittings (ΔE_Q = 1.6 and 2.4 mm/s).[47] (One failing of the synthetic analogues thus far is their inability to attain the larger ΔE_Q values observed in the proteins.) The inequivalence of the iron sites now corroborated by resonance Raman and Mössbauer data casts further doubt on the proposal that the B2 subunit of ribonucleotide reductase contains one dinuclear iron unit coordinated to protein ligands at the interface of the two equivalent polypeptide chains.[14] The present data support the model proposed by Lynch et al. that does not impose any symmetry on the dinuclear site and consists of one dinuclear unit per polypeptide chain.[48]

Acknowledgment. We thank Professor J. D. Britton for his assistance and expertise with the structure determinations. This work was supported by grants from the National Institutes of Health (Grant No. GM-38767, L.Q.; Grant No. GM-18865, J.S.-L.) and the Louisiana Education Quality Support administered by the Board of Regents of the state of Louisiana and by the donors of the Petroleum Research Fund, administered by the American Chemical Society (C.J.O.).

Supplementary Material Available: Atomic numbering scheme (Figure 1), tables of crystallographic parameters (S1), atomic coordinates (A–C), bond lengths and angles (S2–S4), and anisotropic thermal parameters (S5–S7), fits of the magnetic susceptibility data (Figures S2–S5) for **1–3** and **11** (64 pages); listing of structure factor amplitudes (S8–S10) for **1–3** (65 pages). Ordering information is given on any current masthead page.

(46) Sahlin, M.; Ehrenberg, A.; Gräslund, A.; Sjöberg, B.-M. *J. Biol. Chem.* **1986**, *261*, 2778–2780.
(47) Atkin, C. L.; Thelander, L.; Reichard, P.; Lang, G. *J. Biol. Chem.* **1973**, *248*, 7464–7472.
(48) Lynch, J. B.; Juarez-Garcia, C.; Münck, E.; Que, L., Jr. *J. Biol. Chem.* **1989**, *264*, 8091–8096.